Hot and Cold Clusters: Photodissociation of $Sr^+(CH_3OD)_n$ through Vibrationally Excited Intermediates

James I. Lee[†] and James M. Farrar*

Department of Chemistry, University of Rochester, Rochester, New York 14627

Received: July 23, 2002; In Final Form: October 16, 2002

This study presents photodissociation branching ratio data for clusters formed by solvation of Sr^+ with CH_3-OD molecules. The primary photoproducts in clusters with one to four solvent molecules are evaporative ligand loss, C−O bond cleavage to form $SrOD^+$, and O−D bond cleavage, forming $SrOCH_3^+$. Careful analysis of the mass spectra of products and unphotolyzed parent ions as a function of laser fluence shows that clusters that lose a single solvent molecule may absorb additional photons, undergoing subsequent solvent evaporation and chemical reaction. Cluster ions formed by loss of one or more solvent molecules are vibrationally excited, and their subsequent photolysis products reveal strong enhancement of reactive channels involving D-atom loss and C−O bond cleavage relative to cold clusters produced directly by supersonic expansion. In addition to determining branching ratios for the products of vibrationally excited clusters, the study reveals that these hot clusters also have dissociation spectra that are strongly red-shifted relative to their cold counterparts.

Introduction

Mass spectrometry and optical spectroscopy of size-selected cluster ions are important methods for understanding solvation phenomena, especially the manner in which each successive solvent molecule contributes to the establishment of the properties of bulk solutions.[1] The issue of solvation in open-shell ions such as the alkaline earth elements is particularly rich because of the possibility of coupling the electronic energy of the atomic ion core with reactive processes involving solvent degrees of freedom.[2−4] Because the excitation energies of electronic states based on the strongly allowed valence transitions in the alkaline earth ions exceed their electrostatic binding energies with polar solvents such as H_2O, CH_3OH, and CH_3NH_2, those couplings can lead to dissociation by cleavage of specific bonds within the solvent as well as by the simpler process of solvent evaporation.[5−11] Those processes can occur both on excited-state surfaces and on the ground-state surface following internal conversion. The local electronic environment of the metal ion valence electron provides detailed spectroscopic information about excited state and ground-state processes.

Experiments that resolve multiple product formation channels are especially valuable in distinguishing between ground-state and excited-state pathways in solvated metal ion cluster photochemistry. Often, thermochemical data provide clear explanations for why one product channel is favored over another. Experiments in high-pressure[12−14] and high-temperature[15,16] mass spectrometry in conjunction with theoretical binding energy calculations[17−20] are indispensable in estimating reaction threshold energies. However, the observation of reaction channels that are inconsistent with the absorption of single photons is a frequent occurrence but one that is often ignored in quantitative interpretation of experimental data.

Sequential photon absorption effects have been discussed explicitly in a number of systems related to the present study.

Tyndall and Jackson showed that both one- and two-photon processes occur in the photodissociation of $Mo(CO)_6$.[21] While investigating $Ca^+(H_2O)_n$, Sanekata et al. found that above an energetic threshold, a single-photon process creates the $CaOH^+$ product, but below that threshold, a two-photon process is required.[22] Similar behavior was also observed in the Mg^+-$(H_2O)_n$ systems.[10,23] In related work, France et al.[24] investigated the photolysis of $Mg^+(CH_3OH)_n$ for $n = 1−6$. In the singly solvated cluster, both $MgOH^+$ and Mg^+, the expected products of single-photon absorption, are formed, but the authors also reported small amounts of MgO^+ and CH_3^+. Energetic considerations indicate that these latter channels require at least two 350 nm photons.

In a recent publication from our laboratory,[25] we reported photolysis frequency-dependent photodissociation spectra for $Sr^+(CH_3OD)_n$, with $n = 1$ to 4. The data showed that dissociation in these species occurs through excited electronic states based on the *5p* and *4d* orbitals of Sr^+. Product formation occurs by simple solvent evaporation and also by two distinct chemical reactions. In the first reactive process, a C−O bond in the solvent is cleaved to eject a CH_3 fragment, resulting in clusters of the form $SrOD^+(CH_3OD)_m$, and *m*, the number of solvent molecules, is at least one fewer in number than in the parent. In the second reactive dissociation channel, an O−D bond is cleaved, ejecting a deuterium atom and producing clusters of the form $SrOCH_3^+(CH_3OD)_m$, with similar restrictions on *m*, the solvent number. The reaction channels and their endoergicities are summarized here:

$$Sr^+(CH_3OD) \rightarrow Sr^+ + CH_3OD \quad \Delta H = 23 \text{ kcal mol}^{-1} \quad (1)$$

$$\rightarrow SrOD^+ + CH_3 \quad \Delta H = 10 \text{ kcal mol}^{-1} \quad (2)$$

$$\rightarrow SrOCH_3^+ + D \quad \Delta H = 22 \text{ kcal mol}^{-1} \quad (3)$$

Following the notation introduced in our previous paper,[25] we refer to reaction 1 as the −L channel, reaction 2 as the −Me channel, and reaction 3 as the −D channel. The nature of the

* Author to whom correspondence should be addressed.
† Present address: Stanford Research Systems, 1282 Reamwood Ave., Sunnyvale, CA 94089.

Hot and Cold Clusters

J. Phys. Chem. A, Vol. 106, No. 49, 2002 **11883**

electronic states leading to fragmentation by loss of a single solvent molecule was discussed in terms of the branching ratios for photolysis of the singly solvated species $Sr^+(CH_3OD)$.

In this paper, we report branching ratio data for dissociation of $Sr^+(CH_3OD)_n$, $n = 2-4$. The primary photochemical channels 1–3, which we will refer to as first-generation products, are observed both as indicated above, and also in combination with the evaporation of additional solvent molecules. We illustrate that these combination channels result from sequential photon absorption, in which daughter ions formed by solvent evaporation from the parent ion absorb additional photons, creating higher generations of fragments by evaporation and reaction, channels 1–3.

The notation we employ for these combination processes is a generalization of that developed for the primary processes: the channels are denoted by $-(L + mL)$, $-(Me + mL)$, and $-(D + mL)$, where the coefficient m indicates the number of additional solvent molecules lost by the parent ion. The photoproducts denoted by this notation depend explicitly on the identity of the parent ion. Treatment of the experimental data in terms of sequential absorption results in significant simplification of the analysis, allowing us to focus on the first-generation products of channels 1–3, irrespective of cluster size. The analysis also allows us to recover the dissociation spectra of clusters with significant amounts of vibrational excitation. These spectra, as well as the modifications to branching ratios that accompany vibrational excitation in the precursor parent ion, provide additional insights into the dissociation processes.

Experimental Section

The experimental apparatus for these experiments has been described in detail previously.[26] Methanol vapor seeded in He carrier gas at 1.5 atm is adiabatically expanded through a pulsed valve into a laser vaporization ion source, where strontium metal is ablated and ionized by focused second harmonic radiation from a Nd^{3+}:YAG laser. The seeded vapor passes through the Sr^+ plasma, creating a distribution of cluster sizes, $Sr^+(CH_3OD)_n$, which are collisionally cooled as they travel in a supersonic expansion down a channel into the source chamber. The internal temperatures of these clusters are a few tens of K.[26] Following mass selection by a Wiley–McLaren-type time-of-flight mass spectrometer, the clusters are photolyzed by radiation that crosses the cluster beam at the spatial focus. This radiation is provided by a narrow bandwidth (~0.2 cm^{-1}) singly resonant optical parametric oscillator, OPO, pumped by the third harmonic of an injection-seeded Nd^{3+}:YAG laser running at 10 Hz. The OPO signal wave tuning range is from 440 to 690 nm and the idler wave tunes from 730 to 1830 nm. Frequency doubling the signal wave produces radiation from 220 to 345 nm, while the range from 366 to 450 nm is accessed by doubling idler frequencies. Photodissociation laser power was kept at a constant value of 1 mJ/pulse; for a laser spot size of 0.5 cm diameter, the fluence corresponds to 1.2 mJ cm^{-2}. The distributions of photodissociation products and unphotolyzed reactant ions are separated using a reflectron-type mass spectrometer. A set of off-axis microchannel plates detects and amplifies the signal.

The upper panel of Figure 1 shows a mass spectrum of products and unphotolyzed reactant ions for $Sr^+(CH_3OD)_2$ at 588 nm, illustrating the formation of the first-generation products $-L$, $-Me$, and $-D$. The reflectron is operated in the "hard reflection" mode in this scan, and thus the parent and fragment intensities are interleaved. The peak labeled "P" corresponds to the intensity of residual (undissociated) $^{86}Sr^+(CH_3OD)_2$, and

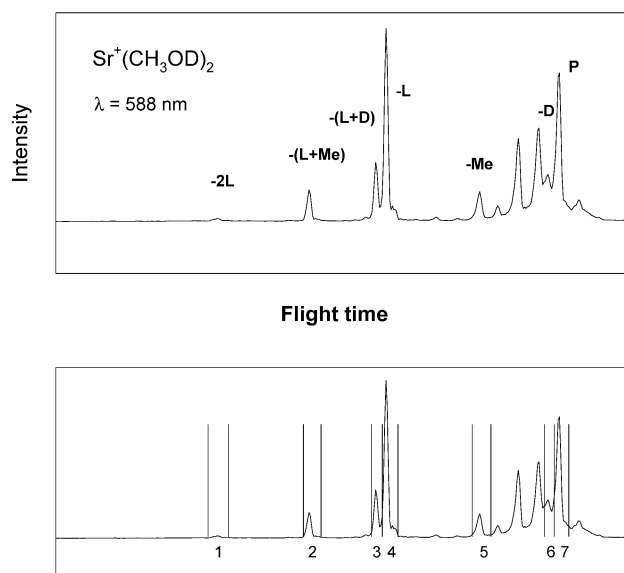**Figure 1.** Upper panel: Mass spectrum of fragments and unphotolyzed $Sr^+(CH_3OD)_2$ parent ions at 588 nm (17007 cm^{-1}). The parent ion is denoted P; the first-generation fragments are labeled $-D$, $-Me$, and $-L$; and the second-generation fragments are labeled $-(D + L)$, $-(Me + L)$, and $-2L$. Lower panel: The time windows for signal integration (1) $-$ (7) correspond to the analysis of eqs 4–6 in the text.

six fragments labeled according to our convention are also shown. An analysis of such mass spectra in which the intensities are interpreted in terms of primary one-photon and sequential multiple-photon absorption is described in the next section of the paper.

Results

The experimental data are in the form of product mass spectra of size-selected clusters taken as a function of the photolysis wavelength and exemplified by the data of Figure 1. The total dissociation signal at a given photolysis wavelength is obtained by integration of the intensities of first-generation fragments and combination channels. As described in the following Data Analysis section, for the computation of product branching ratios, we treat all combination channels arising from cold clusters as secondary (or tertiary) detection of the first-generation ligand loss channel. This treatment reduces the number of unique channels to three, i.e., $-D$, $-Me$, and $-L$, for any cluster size. In the top panel of Figure 2, the total dissociation signal for $Sr^+(CH_3OD)$ clusters produced by supersonic expansion is plotted as a function of photolysis frequency in units of cm^{-1}; the lower panel shows the fraction of the first-generation dissociation signal associated with each of the three primary photochemical channels. As described in previous work from our laboratory,[25] Figure 2 shows that in the extreme red end of the dissociation spectrum, deuterium atom loss is the primary decay channel, dominating methyl loss and solvent evaporation by nearly an order of magnitude. As the photolysis wavelength decreases, the methyl loss channel increases in importance, dominating the branching ratio in the two highest energy dissociation bands.

Figure 3 plots the total dissociation signal and the branching fractions for first-generation fragments for the $Sr^+(CH_3OD)_2$ clusters produced by supersonic expansion, i.e., "cold" dimers. Figures 4 and 5 present similar results for $Sr^+(CH_3OD)_3$ and $Sr^+(CH_3OD)_4$, the cold trimer and tetramer, respectively. The upper panels of each figure show the total dissociation spectra for the parent ion, and the lower panels of each figure give first-
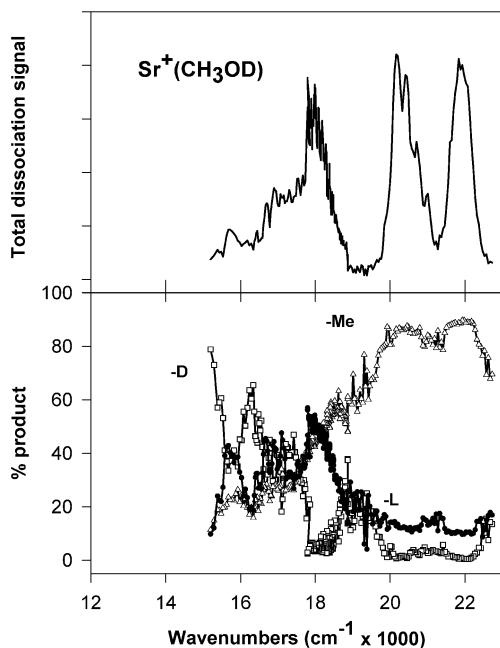
Figure 2. Upper panel: $Sr^+(CH_3OD)$ cold monomer total photodissociation signal for formation of all product channels. Arbitrary intensity scale. Lower panel: branching fractions for the first-generation fragments −D, −Me, and −L.
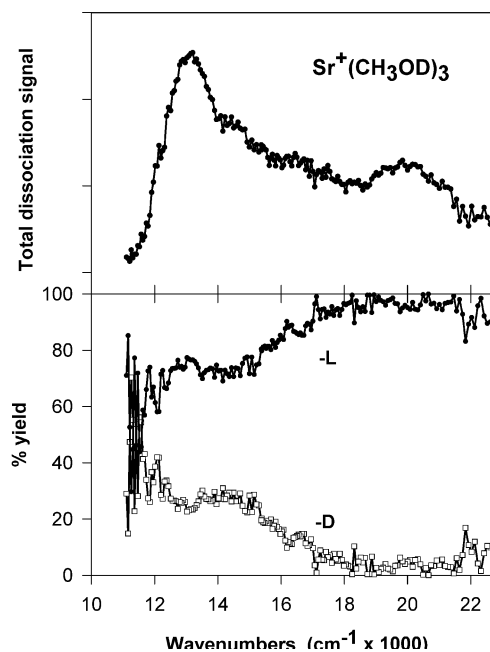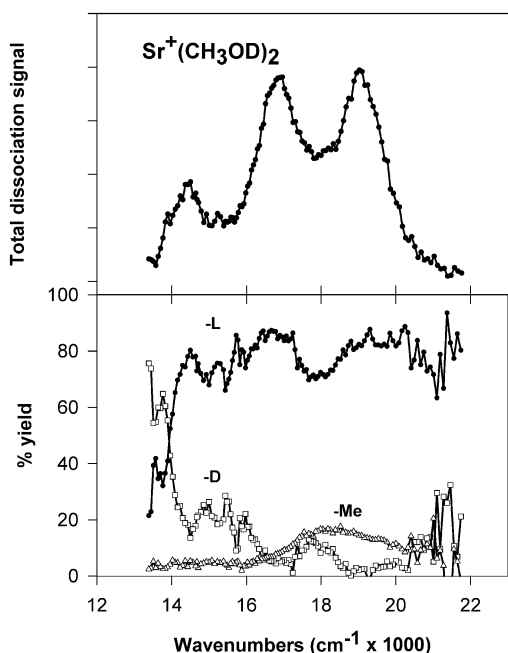

Figure 4. Upper panel: $Sr^+(CH_3OD)_3$ cold trimer total photodissociation signal for formation of all product channels. Arbitrary intensity scale. Lower panel: branching fractions for the first-generation fragments −D and −L.
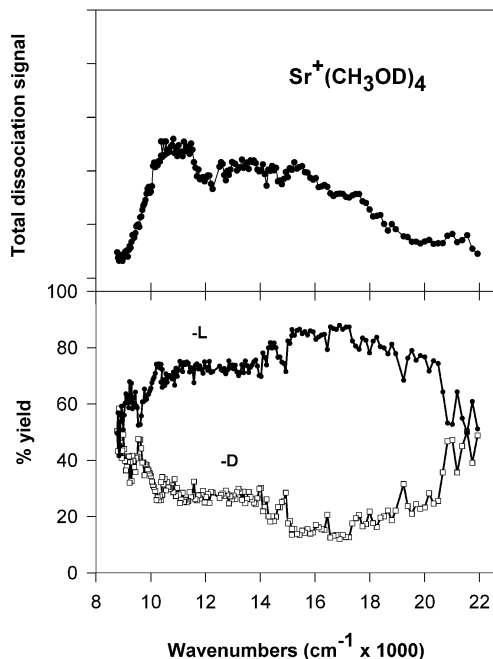

Figure 3. Upper panel: $Sr^+(CH_3OD)_2$ cold dimer total photodissociation signal for formation of all product channels. Arbitrary intensity scale. Lower panel: branching fractions for the first-generation fragments −D, −Me, and −L.

Figure 5. Upper panel: $Sr^+(CH_3OD)_4$ cold tetramer total photodissociation signal for formation of all product channels. Arbitrary intensity scale. Lower panel: branching fractions for the first-generation fragments −D and −L.

generation product yields corresponding to channels −D, −Me, and −L relative to the appropriate parent ion. Both the cold trimer and tetramer demonstrate only decay by deuterium atom loss and solvent evaporation, with the latter channel dominating in both clusters. Decay by methyl loss is absent in both clusters. At low photolysis wavelengths, the −L channel increases with increasing photon energy for both clusters, but the trimer decays exclusively through the −L channel at the blue end of the spectrum, while the −D channel regains signal strength in this spectral range for the tetramer.

Data Analysis

In the dimer and larger clusters, the "combination" channels, in which the primary processes (1) − (3) are accompanied by solvent loss, become accessible. To estimate the enthalpy change for the −(D + L) combination channel, we simply sum the −L and −D enthalpies to yield 45 kcal/mol, which we will use as an upper limit to the enthalpy change. The same estimation method yields a reasonable upper bound for the enthalpy change of the −(L + Me) channel in $Sr^+(CH_3OD)_2$ as 33 kcal/mol.

Hot and Cold Clusters

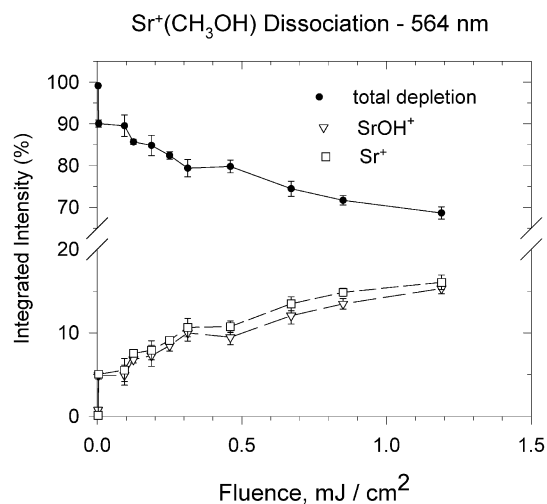*J. Phys. Chem. A, Vol. 106, No. 49, 2002* **11885**

Sr⁺(CH₃OH) Dissociation - 564 nm

Figure 6. Measured fluence dependence of parent ion depletion and daughter ion growth for photolysis of $Sr^+(CH_3OH)$ at 564 nm. The photolysis cross section is 4×10^{-16} cm².

The successive metal–ligand bond strengths decrease with increasing cluster size, as both calculation[20] and experiment[6,12,27,28] on the similar $Sr^+(H_2O)_n$ system have shown. The threshold wavelengths for production of a given fragment obtained from the data of Figures 3–5 show a very similar trend in the photolysis energies required to produce ligand loss and deuterium loss in $Sr^+(CH_3OD)_{2-4}$. Significantly, however, the –Me channel is only observed as a first-generation one-photon product in the monomer and dimer, indicating that the barrier to this channel is not lowered by the addition of a third or fourth solvent molecule. The experimental mass spectra show that the number of observed photochemical products increases quickly with cluster size, owing to multiple combination channels. Although the ligand binding energies decrease with increasing cluster size, some of the photodissociation channels in the dimer are not directly accessible with a single photon. Although the importance of internal excitation in cluster ions formed in an evaporative ensemble in the ground electronic state has been discussed in the literature,[29] we have already noted that parent ion clusters produced by supersonic expansion with our current instrument do not have high levels of internal excitation. Clearly, energetics alone are insufficient to explain the appearance of some of the combination channels in the larger clusters. These observations will be discussed in terms of sequential absorption below.

The ligand loss channel in every parent cluster $Sr^+(CH_3OD)_n$ with $n > 1$ produces the n − 1 cluster, which may absorb a second photon to create another set of products chemically identical to those formed by direct photodissociation of $Sr^+(CH_3OD)_{n-1}$. In addition, the cluster packet trajectories are unaffected by photolysis,[30] and thus satisfy the spatial overlap requirement between parent and daughter. As the cluster travels only about 0.4 mm during the 10 ns photolysis pulse, it will not escape the 5 mm diameter spot size before the pulse ends, thus satisfying the criterion for temporal overlap. We must therefore consider the possibility that the products of ligand loss can themselves absorb additional photons. This possibility requires us to view the three product channels displayed in the monomer as displayed again by successively larger parent ions, rather than considering each of the combination products as a distinct reaction.

Measurements of product branching ratios as a function of laser fluence provide quantitative justification for a sequential photon absorption mechanism. For the monomer, Figure 6
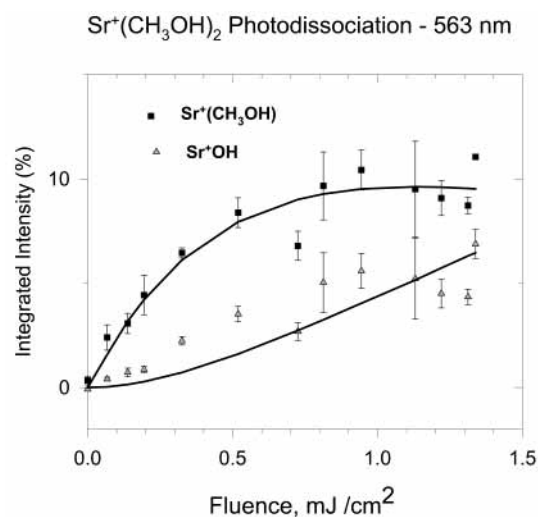
Sr⁺(CH₃OH)₂ Photodissociation - 563 nm

Figure 7. Measured fluence dependence for formation of indicated fragment ions from $Sr^+(CH_3OH)_2$ at a photolysis wavelength of 563 nm. The solid curves are fits to the sequential decay analysis of eqs 6–8 in the text, with cross sections $\sigma_1 = 2 \times 10^{-17}$ cm², $\sigma_2 = 2 \times 10^{-16}$ cm².

demonstrates that the depletion of the parent ion intensity and the corresponding exponential growth of fragment intensities Sr^+ and $SrOH^+$ at a photolysis wavelength of 564 nm. The fluence measurements were conducted with undeuterated solvent; consequently, mass resolution was insufficient to detect the $SrOCH_3^+$ channel produced via hydrogen atom loss. The identical fluence dependences for $SrOH^+$ formation via the –Me channel and Sr^+ via the –L channel indicate that both are formed by single-photon processes. Significantly, the $SrOH^+$ does not show evidence of additional photon absorption.

Figure 7 shows a similar measurement that focuses on the production of fragment ions produced from the dimer, $Sr^+(CH_3OH)_2$, at 563 nm. Two products are observed: the $Sr^+(CH_3OH)$ fragment formed via the –L channel has a fluence dependence consistent with single-photon absorption. The $SrOH^+$ product is consistent with formation via two photons. Since the monomer photochemistry shows that $SrOH^+$ itself does not absorb photons, the scheme for producing $SrOH^+$ must be the two-photon sequential process as follows:

$$Sr^+(CH_3OH)_2 + h\nu \rightarrow Sr^+(CH_3OH)^* + CH_3OH \quad (4)$$

$$Sr^+(CH_3OH)^* + h\nu \rightarrow SrOH^+ + CH_3 \quad (5)$$
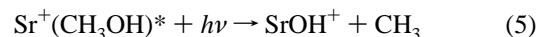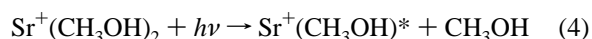
The kinetic scheme for sequential two-photon absorption is analogous to the decay scheme for successive first-order reactions.[31] For sequential photon absorption via the symbolic process $A \xrightarrow{\sigma_1} B \xrightarrow{\sigma_2} C$, the solutions for the number densities of species A, B, and C at the conclusion of a photon pulse of fluence Φ are given as follows:

$$N_A(t) = N_A(0)e^{-\sigma_1 \Phi} \quad (6)$$

$$N_B(t) = \frac{\sigma_1}{\sigma_2 - \sigma_1}N_A(0)[e^{-\sigma_1 \Phi} - e^{-\sigma_2 \Phi}] \quad (7)$$

$$N_C(t) = N_A(0) - N_A(t) - N_B(t) \quad (8)$$

The solid curves shown in Figure 7 are fits of the experimental data to this scheme. The sequential scheme shows that the limiting slope at zero fluence for the first-generation one-photon
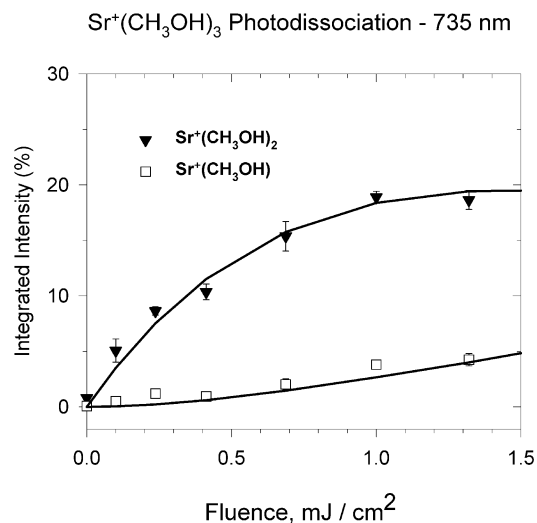
Sr$^+$(CH$_3$OH)$_3$ Photodissociation - 735 nm

Figure 8. Measured fluence dependence for formation of indicated fragment ions from Sr$^+$(CH$_3$OH)$_3$ at a photolysis wavelength of 564 nm. The solid curves are fits to the sequential decay analysis of eqs 6−8 in the text, with cross sections $\sigma_1 = 3 \times 10^{-17}$ cm^2, $\sigma_2 = 7 \times 10^{-17}$ cm^2.

fragment is finite and nonzero, while the corresponding slope for the second-generation fragments formed by two-photon absorption, i.e., SrOH$^+$, is zero. Within the experimental error of the fluence data, these observations are confirmed in the data of Figure 7.

Figure 8 shows fluence data for the two ligand loss channels in the trimer, denoted −L and −2L, forming products Sr$^+$(CH$_3$-OH)* and Sr$^+$(CH$_3$OH)**, respectively. As expected, loss of a single ligand shows a fluence dependence consistent with single-photon absorption, and loss of two ligands shows a fluence dependence properly described by sequential absorption of two photons. Model calculations are shown by the solid curves.

The fluence measurements indicate that the −Me product of photolysis, SrOH$^+$ (or SrOD$^+$), is formed by single-photon absorption and does not undergo additional photon absorption. The SrOCH$_3^+$ species, formed by loss of a hydrogen (or deuterium) atom bound to the oxygen, is chemically similar to SrOD$^+$, in that the Sr−O bond is largely covalent, and would likewise not be expected to absorb an additional visible photon. We expect that clusters formed by single-photon dissociation through the −D and −Me pathways, SrOCH$_3^+$(CH$_3$OD)$_{n-1}$ and SrOD$^+$ (CH$_3$OD)$_{n-1}$, respectively, will not absorb additional photons and participate in additional photodissociation. However, the electrostatically bound Sr$^+$(CH$_3$OD)$_{n-1}$ product is free to absorb another photon and dissociate via one of the three pathways available in the first absorption, creating another group of products. These observations lead us to suggest that the sequential absorption scheme shown in Figure 9, in which a cluster of size n absorbs a photon and decays along one of three reaction pathways, creating the analogous products observed in the monomer, solvated by $n - 1$ ligands, is operative in the Sr$^+$(CH$_3$OD)$_n$ systems.

The consequences of the sequential absorption mechanism can be examined by a more detailed analysis of the experimental data. Specifically, by employing an analysis like that proposed in Figure 9, we expect to extract photodissociation spectra and product branching ratios for Sr$^+$(CH$_3$OD)$_m$ ions prepared by one- and two-photon absorption of cold precursor parent cluster ions. We first consider the experimental data for Sr$^+$(CH$_3$OD)$_2$ as shown in the lower panel of Figure 1, in which signals integrated over appropriate time windows are labeled with an
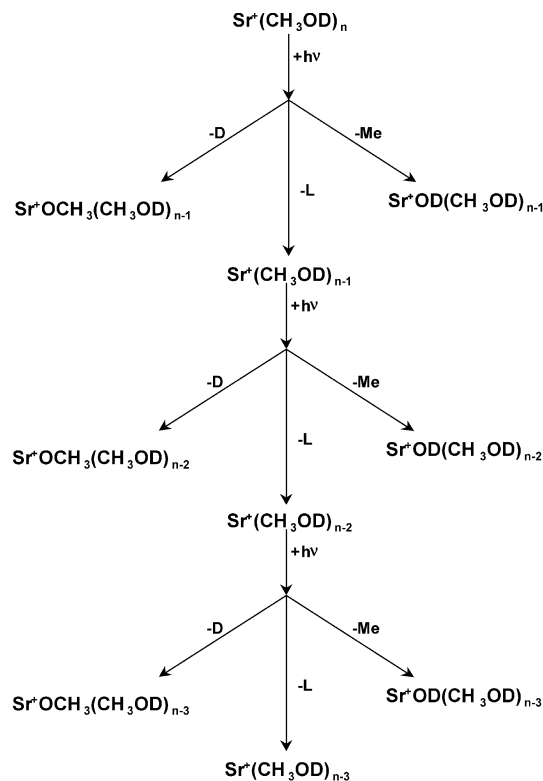

Figure 9. Schematic depiction of the proposed sequential absorption mechanism, illustrating that higher-order generations are accessed only through Sr$^+$−(CH$_3$OD)$_m$ species.

integer index from 1 to 7, with fragments corresponding to channels 1−6, residual parent to channel 7. Conservation of charge requires that the sum of the fragment intensities and the residual parent ion intensity should equal the initial charge in the cluster. Letting X_m represent the area of the mass spectral peak for channel m, i.e., the charge of channel m as indicated in Figure 1, the sum $\Sigma_n X_n$ over fragments and residual parent ion represents the total charge in the ion packet. The total dissociation signal is the ratio of all the fragment intensities ($n = 1−6$) to the total charge in the packet:

$$\text{total photodissociation signal} = \{\sum_{n=1}^{6} X_n\}/\{\sum_{n=1}^{7} X_n\} \quad (9)$$

The normalized signal for any dissociation channel j, $j = 1−6$, is given as

$$\text{channel } j \text{ signal} = \{X_j\}/\{\sum_{n=1}^{7} X_n\} \quad (10)$$

As required by energy conservation, it is appropriate to view the combination channels in Figure 1, denoted by −2L, −(L + Me), and −(L + D), as arising from absorption of a second photon by the monomer. We may therefore treat the first-generation cluster denoted by −L as the residual parent of the combination channels. Making that assumption, the total photodissociation signal arising from monomers produced by single-photon dissociation of cold dimers is given by the following equation:

$$\text{total dissociation signal, monomer from dimer} =$$

$$\{\sum_{n=1}^{3} X_n\}/\{\sum_{n=1}^{4} X_n\} \quad (11)$$

Hot and Cold Clusters

J. Phys. Chem. A, Vol. 106, No. 49, 2002 **11887**

The signals from the individual second-generation fragment channels are normalized to the total charge of the residual parent. Thus, the ligand loss peak is treated as the residual parent ion for the subsequent photon absorption event, and the integral over this time window plus the integral over each of the combination channel daughter windows is treated as the total ion flux for the intermediate absorption event. We use the same technique in the larger clusters to higher order.

This mechanism corresponds to sequential absorption of single photons by different species, i.e., successive generations of fragment ions. The mechanism is qualitatively different from one proposed by Fuke and co-workers in which the same parent ion is hypothesized to absorb two photons sequentially.[9,10,22] These workers proposed a sequential absorption mechanism to account for formation of $MgOH^+$ $(H_2O)_n$ products at photolysis energies below their estimated thermodynamic thresholds. Such a mechanism is likely in the case of Mg^+-centered transitions, but not those based on Sr^+, because the electronic states of the former are ordered ^2S, ^2P, ^2D with respect to energy, their energy spacings are comparable, and adjacent levels are coupled by dipole-allowed transitions. If the sequential absorption mechanism for parents and higher generations of fragment ions proposed here is valid, we expect to recover features in the absorption spectrum of the intermediate that are similar to the structures observed when the same cluster size is interrogated directly. However, the internal energy distributions of clusters produced by dissociation are expected to be significantly different from those of cold clusters. We expect the differences in internal state distributions to reveal themselves in significant spectral shifts and in modifications to the product channel distributions as a function of photolysis frequency.

Figure 10 shows the intensity distribution of the second-generation fragments from $Sr^+(CH_3OD)_2$ normalized by treating the −L daughter ion, i.e., $Sr^+(CH_3OD)^*$, as the residual parent. In essence, Figure 10 plots the one-photon photofragment signal for monomer ions produced by single-photon dissociation of cold dimer ions. As described in the Discussion section, we expect the nascent monomers created by photodissociation to be internally excited, and thus we attribute the spectrum to vibrationally "hot" monomer ions. The notation $Sr^+(CH_3OD)^*$ indicates that the parent ion yielding the spectrum is itself produced by photolysis. The bottom panel of Figure 10 plots the branching fractions of the −D, −Me, and −L products of these hot monomers. The distributions are markedly different from those of the "cold" monomer, with a significant enhancement of reaction channels over solvent evaporation.

Figure 11 presents the results of the sequential absorption analysis to the fragmentation products of $Sr^+(CH_3OD)$ produced by sequential loss of two ligands from cold $Sr^+(CH_3OD)_3$ clusters. The branching ratios for the third-generation fragments −D, −Me, and −L relative to the monomer, i.e., −(D + 2L), −(Me + 2L), and −3L relative to the cold trimer, are plotted in the bottom panel of this figure. The total dissociation spectrum for this species, denoted $Sr^+(CH_3OD)^{**}$, is significantly red-shifted and broadened relative to $Sr^+(CH_3OD)$ and $Sr^+(CH_3OD)^*$. The maximum intensity in this spectrum occurs nearly 5000 cm^{-1} to the red of the lowest frequency feature in the $Sr^+(CH_3OD)^*$ spectrum. The enhancement of reaction channels over evaporation, which first evidenced itself in the $Sr^+(CH_3OD)^*$ spectrum, is even more apparent in the $Sr^+(CH_3OD)^{**}$ spectrum. Of particular note is the fact that the favoring of the −D channel over the −Me channel is especially pronounced in the spectral region below 16000 cm^{-1}, where cold $Sr^+(CH_3OD)$ and "hot" $Sr^+(CH_3OD)^*$ have little dissociation signal.

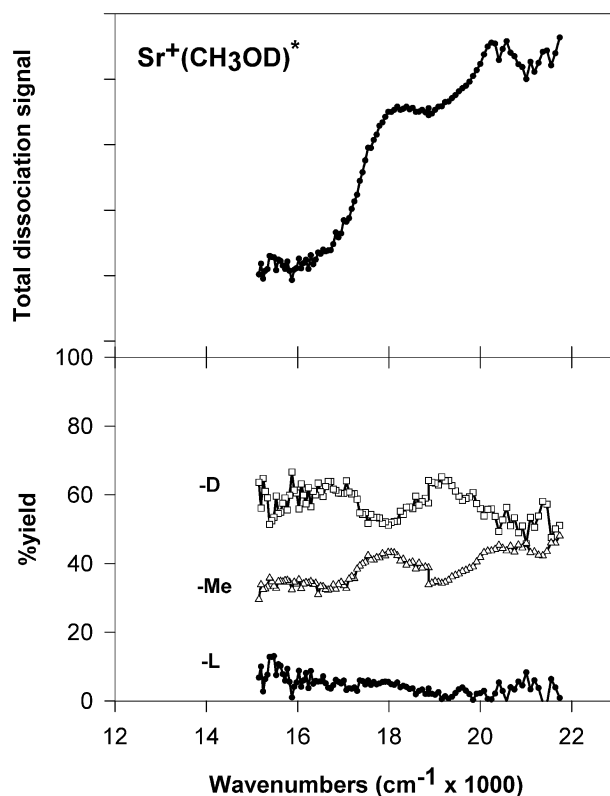**Figure 10.** Upper panel: $Sr^+(CH_3OD)^*$ hot monomer total photodissociation signal for formation of all product channels. Arbitrary intensity scale. The signal at each photolysis wavelength arises from the first-generation fragments coming from $Sr^+(CH_3OD)^*$ produced by single-photon dissociation of $Sr^+(CH_3OD)_2$. Lower panel: branching fractions for the −D, −Me, and −L channels relative to the residual parent $Sr^+(CH_3OD)^*$ arising from single-photon absorption in the dimer.

Figure 12 presents the results of sequential analysis to the fragments of $Sr^+(CH_3OD)_2^*$ formed by the −L channel in the trimer, and Figure 13 presents comparable data for the −D, −Me, and −L channels from trimer ions, denoted $Sr^+(CH_3OD)_3^*$, formed by single-photon loss of a solvent molecule in the tetramer. The total dissociation spectra themselves are broad and featureless. The "hot" dimer, $Sr^+(CH_3OD)_2^*$, shows significant enhancement of reaction over evaporation relative to its cold counterpart. In both hot and cold trimer, the −L channel is dominant; in the cold trimer, the −Me channel does not appear, but the hot trimer always shows a significant component of C−O bond cleavage, reaching ∼10% of the total dissociation signal at the highest photolysis frequencies.

We note an important implication of this data treatment. First, the total dissociation curves presented in the Results section are completely unaffected by this analysis. For simplicity, one can think of the sequential absorption channels as being merely secondary (or tertiary) detection of the initial absorption event. This idea of secondary detection can be used to our advantage by allowing us to consider fewer product channels. The first intermediate in any cluster dissociation is the single ligand loss channel. Each subsequent absorption event can be treated as secondary detection of this channel, just as any channel can be treated as detection of the initial absorption event to the appropriate order. With all combination channels treated as secondary detection of the ligand loss channel, there are only three channels to consider in each cluster: −D, −Me, and −L. This is a very powerful data reduction; we deal with three channels for each cluster size instead of as many as seven in some clusters. Finally, the most intriguing aspect of this
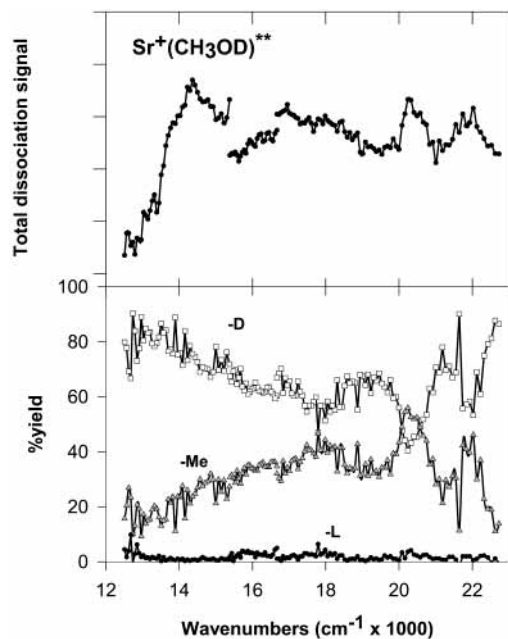
Figure 11. Upper panel: $Sr^+(CH_3OD)^{**}$ "superhot" monomer total photodissociation signal for formation of all product channels. Arbitrary intensity scale. The signal at each photolysis wavelength arises from the first-generation fragments coming from $Sr^+(CH_3OD)^{**}$ produced by sequential two-photon dissociation of $Sr^+(CH_3OD)_3$. Lower panel: branching fractions for the $-D$, $-Me$, and $-L$ channels relative to the residual parent $Sr^+(CH_3OD)^{**}$ arising from two-photon absorption in the trimer.

Figure 12. Upper panel: $Sr^+(CH_3OD)_2^*$ hot dimer total photodissociation signal for formation of all product channels. Arbitrary intensity scale. The signal at each photolysis wavelength arises from first-generation fragments from $Sr^+(CH_3OD)_2^*$ produced from one-photon dissociation of $Sr^+(CH_3OD)_3$. Lower panel: branching fractions for the $-D$, $-Me$, and $-L$ channels relative to the residual parent $Sr^+(CH_3OD)_2^*$ arising from single-photon absorption in the trimer.

treatment is the possibility of gleaning spectroscopic and dynamical insight into the vibrationally excited intermediates and comparing these data to their vibrationally cold counterparts.
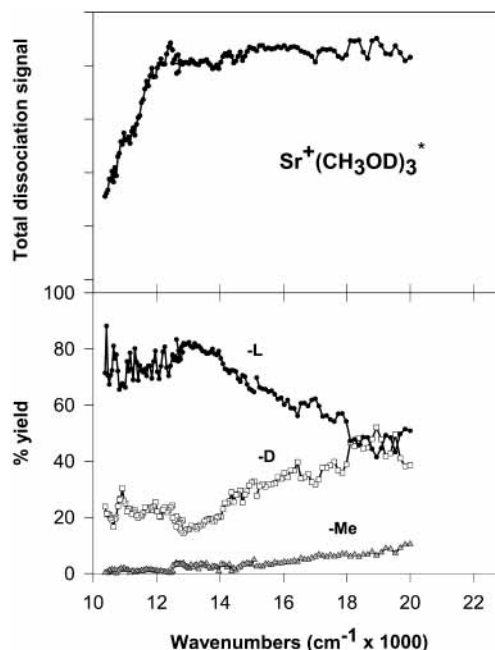

Figure 13. Upper panel: $Sr^+(CH_3OD)_3^*$ hot trimer total photodissociation signal for formation of all product channels. Arbitrary intensity scale. The signal at each photolysis wavelength arises from first-generation fragments from $Sr^+(CH_3OD)_3^*$ produced from one-photon dissociation of $Sr^+(CH_3OD)_4$. Lower panel: branching fractions for the $-D$, $-Me$, and $-L$ channels relative to the residual parent $Sr^+(CH_3OD)_3^*$ arising from single-photon absorption in the tetramer.

Discussion

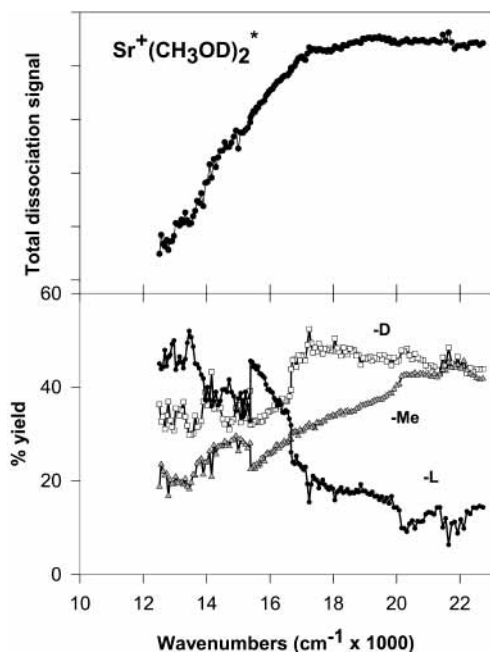To understand the implications of the sequential photon analysis on the total photodissociation signal and the size-dependence of the product branching ratios, we use results for the simplest dissociation system, cold $Sr^+(CH_3OD)$ produced by supersonic expansion, as a baseline. Those results, shown in Figure 2, indicate that O–D bond cleavage dominates the dissociation in the lowest frequency range of the spectrum, where the excited states are primarily based on excitation of atomic ion $4d\pi$-states.[5,20] As states based on Sr^+ $5p\pi$ orbitals are excited at higher frequencies, C–O bond cleavage becomes the dominant reaction channel. The data suggest that electronic states based on the Sr^+ $4d\pi$ orbitals allow efficient internal conversion to regions of the ground-state surface that facilitate the deuterium atom migration, while the Sr^+ $5p\pi$ orbitals have appropriate overlap with the C–O σ^* antibonding orbital.

The "bond stretching attraction" model described by Hertel[32] provides the basis for understanding the dissociation dynamics in alkaline earth ion complexes, particularly the transfer of reactant electronic energy into product vibrational excitation. This model assumes that an intramolecular bond in the solvent lengthens in the excited electronic state of the cluster, creating a potential energy curve crossing between the ground and excited states. As the molecule samples the excited-state surface, the crossing seam is eventually encountered and the molecule returns to the ground electronic state. This internal conversion (IC) results in electronic to vibrational energy transfer and subsequent decay on the ground-state surface. Although ab initio calculations to probe important regions of the potential surfaces for the Sr^+-based reactions have not been carried out to our knowledge, Kleiber and co-workers have performed experimental and theoretical studies on related Mg^+ systems that probe the nature of the key interactions.[33-36] Their work shows clearly that conical intersections between excited states and the ground state facilitate dissociation and resultant internal excitation of

Hot and Cold Clusters

J. Phys. Chem. A, Vol. 106, No. 49, 2002 **11889**

the fragments. Those studies lend strong support to the applicability of the bond-stretching attraction model to alkaline earth−solvent clusters.

According to the expectations of the "bond stretching attraction" model, the products of the photodissociation event are vibrationally hot. If these hot products undergo the absorption of an additional photon, it is plausible to assume that yet more internal energy will be deposited in the products from the second dissociation event. On that basis, we would expect the dissociation spectrum of the "hot" monomer, $Sr^+(CH_3OD)^*$, to reflect that internal excitation, and the spectrum of $Sr^+(CH_3OD)_2^{**}$, referred to as "superhot" monomer, to reflect an even higher level of internal excitation. A comparison of the dissociation spectra of monomer cluster ions prepared with three very different internal energy distributions would be expected to reveal the effects of those differences. It is especially interesting to consider the spectra of $Sr^+(CH_3OD)$, $Sr^+(CH_3OD)^*$, and $Sr^+(CH_3OD)^{**}$, in Figures 2, 10, and 11, respectively. Note in particular the structure that is recovered from the hot and superhot internally excited monomer data taken from the dimer and trimer precursors, respectively. The $4d\sigma$ and $5p\pi$ bands[5] shown in the cold monomer spectrum (Figure 2) are clearly still visible in Figure 10, the "hot" monomer spectrum extracted from the dimer data. The spectrum is broadened, with significant red-shifting expected for hot bands, particularly in the "superhot" monomer, as predicted by the model. Even more striking is the fact that we can still recover structure in the superhot monomer data extracted from the trimer. As shown in Figure 11, the $5p\pi$ bands are again clearly visible at 20 000 and 21 500 cm^{-1}, and it is the −Me channel in all three spectra that carries the structure. The electronic structure correlation provides very telling confirmation of the sequential mechanism.

Branching Ratios and Potential Energy Surface Features

The trends in the data show that methyl elimination is not facilitated by solvation, unlike the −D and −L channels. This observation is consistent with ab initio calculations on $Mg^+(CH_3OH)$ that show both the −H and −L reactions are less endothermic in larger clusters.[8] In analogy with crossed beam work on Ba^* with methanol,[37] in which the hydroxyl hydrogen atom loss channel is observed as the exclusive product, despite the lower exergicity for C−O cleavage, we expect the −D channel to proceed by facile D-atom migration. The −Me channel must be concerted, proceeding through a three-member transition state in which the C atom is sp^3 hybridized and the C−O bond is nearly broken. Solvation may stabilize the $SrOD^+$ product, but the potential energy barrier for such a reaction will remain substantial. While the endothermicity to both the −D and −L channels is lowered by solvation, the −Me channel becomes relatively unfavorable with increasing cluster size and is no longer exhibited once $n = 3$.

A consideration of the role of cluster vibrational excitation provides additional support for the picture discussed in the preceding paragraph. Reactant vibrational excitation is often effective in surmounting potential energy barriers to reaction,[38−41] principally under conditions where the excitation induces molecular motion along critical reaction coordinates. As indicated in Figures 2, 10, and 11, an increase in cluster internal excitation preferentially enhances the cross sections for the −D and −Me reactions that require cleavage of covalent bonds in the solvent. Figures 10 and 11 show that the −D channel is significantly enhanced in all ranges, surpassing the −Me channel. The difference in enhancement of −D and −Me is consistent with the difference in barrier height between the

channels. While both channels are enhanced relative to the branching ratios observed in the cold monomer, the −D channel is much more strongly affected. That difference is particularly striking in Figure 11, where the dissociation cross section in the spectral range below 15000 cm^{-1} must arise from highly vibrationally excited monomers. In that spectral region, the −D channel becomes increasing important as the photolysis frequency decreases, requiring higher levels of reactant internal excitation. Although the dynamical origins of this enhancement are not understood at present and will require theoretical explication, it is sensible to attribute the enhancement of O−D bond cleavage with enhanced D-atom migration associated with O−D vibrational excitation.

Dissociation of vibrationally excited dimers (Figure 12) also results in dramatic changes in the branching ratios relative to the cold dimer. There is obvious competition between the ligand loss channel and the intracluster reaction channels. Both intracluster reaction channels increase roughly monotonically with increasing photolysis energy. However, the ligand loss channel, which increases along with the intracluster reaction channels up to ∼16000 cm^{-1}, steadily drops after that point. At low photolysis energies, the barriers for the −D and −Me channels cause all three decay products to exhibit the same behavior. However, the production of the more stable hydroxide (from −Me) and methoxide (from −D) outweighs formation of the less stable ligand loss product when barriers become less critical to reaction as the photolysis energy increases.

In the spectra of the cold trimer and tetramer, we observe trends similar to those discussed in the smaller clusters. Figures 4 and 5 show that the relatively minor −D channel increases in importance in the lowest energy portion of the cold spectra, again probably corresponding to enhanced IC to the ground electronic state via low-lying d orbitals. Both in the hot dimer and hot trimer, the ligand loss channel strongly dominates the branching ratio at low photolysis energy. With increasing photolysis energy, the −D channel increases at the expense of the −L channel. However, that effect is much more dramatic in the dimer (Figure 12). The −D and −L channels in the hot trimer spectrum (Figure 13) are of comparable intensity at the high energy end of the spectrum, but −L dominates with decreasing photolysis energy. This trend can be explained by the decreased ligand binding energies with increasing cluster size. Qualitatively, the behaviors of the hot dimer and trimer spectra are similar, but in the trimer case, the effective endothermicity to ligand loss has been decreased, making the channel dominant over a broader photolysis energy range. Note that the −Me channel is only weakly accessed in the hot trimer spectrum (Figure 13) however, and that the −Me channel is not exhibited in the cold spectra of either the trimer (Figure 4) or tetramer (Figure 5). The sequential mechanism helps explain this interesting selectivity. Note that while the −Me channel is not observed in the trimer and tetramer, both clusters display loss of −(L + Me). In terms of sequential absorption, this channel corresponds to methyl loss from a hot dimer and trimer, respectively. Likewise, the tetramer displays −(2L + Me), corresponding to methyl loss from a hot dimer. Thus, a cluster must be of dimer size or smaller to eliminate a methyl fragment unless the cluster is already vibrationally excited. This behavior is consistent with our observations on the related $Mg^+(CH_3OD)$ system, in which the −Me channel shuts off for clusters larger than the dimer.[42] As shown earlier, the energy required to access the −L or −D channels drops with increasing cluster size. Once the cluster size reaches three, the endothermicity of these channels is so low relative to the more constant −Me

barrier that they are overwhelmingly favored. It is only when the cluster size is reduced or the cluster becomes vibrationally excited through photodissociation that the endothermicities to −L, −D, and −Me channels become more comparable and elimination of the methyl radical occurs.

Conclusions

We have examined $Sr^+(CH_3OD)_n$ via mass and photodissociation spectroscopy. We formulated a sequential absorption mechanism for the photodissociation pathway in these systems that was validated by our ability to recover the spectral structure of $Sr^+(CH_3OD)$ from $Sr^+(CH_3OD)_2$ and $Sr^+(CH_3OD)_3$ data. Recognizing that this absorption mechanism produces hot intermediates that reabsorb, we recovered the absorption spectra of the intermediates and use these data in interpretation of the photochemical branching ratios. We found that while both intracluster reaction channels proceed over a potential energy barrier, only the deuterium atom elimination barrier is lowered by solvation. On the basis of our data, we conclude that the deuterium elimination occurs through a H (D) migration mechanism while methyl loss must proceed via a metal atom insertion followed by isomerization over a potential energy barrier. Theoretical calculations on this system will be very important, not only for deeper insight into this work, but also for quantification of the barriers to the reaction channels and their behavior with increasing solvation and with reactant vibrational excitation.

References and Notes

(1) Castleman, A. W., Jr.; Bowen, K. H., Jr. *J. Phys. Chem.* **1996**, *100*, 12911−12944.
(2) Kleiber, P. D.; Chen, J. *Int. Rev. Phys. Chem.* **1998**, *17*, 1−34.
(3) Duncan, M. A. *Annu. Rev. Phys. Chem.* **1997**, *48*, 69−93.
(4) Yeh, C. S.; Pilgrim, J. S.; Willey, K. F.; Robbins, D. L.; Duncan, M. A. *Int. Rev. Phys. Chem.* **1994**, *13*, 231−262.
(5) Qian, J.; Midey, A. J.; Donnelly, S. G.; Lee, J. I.; Farrar, J. M. *Chem. Phys. Lett.* **1995**, *244*, 414−420.
(6) Sperry, D. C.; Midey, A. J.; Lee, J. I.; Qian, J.; Farrar, J. M. *J. Chem. Phys.* **1999**, *111*, 8469−8480.
(7) Fuke, K.; Misaizu, F.; Sanekata, M.; Tsukamoto, K.; Iwata, S. *Z. Phys. D*: *At., Mol. Clusters* **1993**, *26*, S180−S182.
(8) Lu, W.; Yang, S. *J. Phys. Chem. A* **1998**, *102*, 825−840.
(9) Misaizu, F.; Sanekata, M.; Tsukamoto, K.; Fuke, K. *J. Phys. Chem.* **1992**, *96*, 8259−8264.

(10) Misaizu, F.; Sanekata, M.; Fuke, K. *J. Chem. Phys.* **1994**, *100*, 1161−1170.
(11) Sanekata, M.; Misaizu, F.; Fuke, K.; Iwata, S.; Hashimoto, K. *J. Am. Chem. Soc.* **1995**, *117*, 747−754.
(12) Tang, I. N.; Lian, M. S.; Castleman, A. W., Jr. *J. Chem. Phys.* **1976**, *65*, 4022−4027.
(13) Harms, A. C.; Khanna, S. N.; Chen, B.; Castleman, A. W., Jr. *J. Chem. Phys.* **1994**, *100*, 3540−3544.
(14) Kochanski, E.; Constantin, E. *J. Chem. Phys.* **1987**, *87*, 1661−1665.
(15) Murad, E. *J. Chem. Phys.* **1983**, *78*, 6611−6613.
(16) Murad, E. *J. Chem. Phys.* **1981**, *75*, 4080−4085.
(17) Bauschlicher, C. W., Jr.; Langhoff, S. R.; Partridge, H.; Rice, J. E.; Komornicki, A. *J. Chem. Phys.* **1991**, *95*, 5142−5148.
(18) Bauschlicher, C. W., Jr.; Partridge, H. *J. Phys. Chem.* **1991**, *95*, 3946−3950.
(19) Sodupe, M.; Bauschlicher, C. W., Jr.; Partridge, H. *J. Chem. Phys.* **1991**, *95*, 9422−9423.
(20) Bauschlicher, C. W., Jr.; Sodupe, M.; Partridge, H. *J. Chem. Phys.* **1992**, *96*, 4453−4463.
(21) Tyndall, G. W.; Jackson, R. L. *J. Phys. Chem.* **1991**, *95*, 687−693.
(22) Sanekata, M.; Misaizu, F.; Fuke, K. *J. Chem. Phys.* **1996**, *104*, 9768−9778.
(23) Misaizu, F.; Sanekata, M.; Tsukamoto, K.; Fuke, K.; Iwata, S. *J. Phys. Chem.* **1992**, *96*, 8259−8264.
(24) France, M. R.; Pullins, S. H.; Duncan, M. A. *Chem. Phys.* **1998**, *239*, 447−457.
(25) Lee, J. I.; Sperry, D. C.; Midey, A. J.; Qian, J.; Farrar, J. M. *J. Phys. Chem. A* **2002**, *106*, 9993−9998.
(26) Donnelly, S. G.; Schmuttenmaer, C. A.; Qian, J.; Farrar, J. M. *J. Chem. Soc., Faraday Trans.* **1993**, *89*, 1457−1465.
(27) Shen, M.; Winniczek, J. W.; Farrar, J. M. *J. Phys. Chem.* **1987**, *91*, 6447−6449.
(28) Shen, M. H.; Farrar, J. M. *J. Chem. Phys.* **1991**, *94*, 3322−3331.
(29) Cabarcos, O. M.; Weinheimer, C. J.; Lisy, J. M. *J. Phys. Chem. A* **1999**, *103*, 8777−8791.
(30) Donnelly, S. G. Photodissociation Studies of Mass Selected Clusters. Doctoral Dissertation, University of Rochester, 1994.
(31) Bateman, H. *Proc. Cambridge Philos. Soc.* **1910**, *15*, 423.
(32) Hertel, I. V. Progress in Electronic-to-Vibrational Energy Transfer. In *Dynamics of the Excited State*; Lawley, K. P., Ed.; Wiley-Interscience: New York, 1982; Vol. L.; p 475.
(33) Chen, J.; Cheng, Y. C.; Kleiber, P. D. *J. Chem. Phys.* **1997**, *106*, 3884−3890.
(34) Chen, J.; Wong, T. H.; Cheng, Y. C.; Montgomery, K.; Kleiber, P. D. *J. Chem. Phys.* **1998**, *108*, 2285−2296.
(35) Cheng, Y. C.; Chen, J.; Ding, L. N.; Wong, T. H.; Kleiber, P. D.; Liu, D.-K. *J. Chem. Phys.* **1998**, *104*, 6452−6459.
(36) Wong, T. H.; Freel, C.; Kleiber, P. D. *J. Chem. Phys.* **1998**, *108*, 5723−5727.
(37) Davis, H. F.; Suits, A. G.; Lee, Y. T.; Alcaraz, C.; Mestdagh, J.-M. *J. Chem. Phys.* **1993**, *98*, 9595−9609.
(38) Crim, F. F. *Science* **1990**, *249*, 1387−1392.
(39) Crim, F. F. *Annu. Rev. Phys. Chem.* **1993**, *44*, 397−428.
(40) Crim, F. F. *J. Phys. Chem.* **1996**, *100*, 12725−12734.
(41) Crim, F. F. *Acc. Chem. Res.* **1999**, *32*, 877−884.
(42) Lee, J. I.; Sperry, D. C.; Farrar, J. M. *J. Chem. Phys.* **2001**, *114*, 6180−6189.